INVISCID AND VISCOUS FLOW MODELLING OF COMPLEX AIRCRAFT CONFIGURATIONS USING THE CFD SIMULATION SYSTEM SAUNA

A J Peace, N E May, M F Pocock, J A Shaw
Aircraft Research Association Ltd,
Manton Lane, Bedford MK41 7PF, UK

Abstract

This paper is concerned with the flow modelling capabilities of an advanced CFD simulation system known by the acronym SAUNA. This system is aimed primarily at complex aircraft configurations and possesses a unique grid generation strategy in its use of block-structured, unstructured or hybrid grids, depending on the geometric complexity of the addressed configuration. The main focus of the paper is in demonstrating the recently developed multi-grid, block-structured grid, viscous flow capability of SAUNA, through its evaluation on a number of configurations. Inviscid predictions are also presented, both as a means of interpreting the viscous results and with a view to showing more completely the capabilities of SAUNA. It is shown that accuracy and flexibility are combined in an efficient manner, thus demonstrating the value of SAUNA in aerodynamic design.

Introduction

It is now normal practice for computational fluid dynamics (CFD) and wind tunnel testing to be used in harmony during an aerodynamic design exercise. It is also the trend in many design tasks for some degree of complex configuration modelling to be undertaken, primarily to aid the understanding of the aerodynamic interaction between aircraft components (eg wing/powerplant). This is now an integral part of the drive towards increased performance and efficiency. The vast majority of these three-dimensional CFD investigations are currently performed using an inviscid modelling approach, commonly with an Euler equation solver. Only a very few viscous solutions are obtained for anything more complex than a wing/body configuration, primarily as few CFD codes have managed to prove, in the design environment, both the required efficiency in mesh generation and accuracy of flow simulation. It is important that current CFD method development addresses this highly challenging area now that the computer hardware for realistically undertaking such computations is on the horizon.

The Aircraft Research Association (ARA) has been highly active in the field of CFD complex configuration modelling since the early 1980s. Pioneering work on the multi-block (block-structured) mesh generation method, including the first demonstration of this technique for external aerodynamic flows[1], was followed by continued development and refinement of the method[2,3], and a number of successful applications in the design environment in the UK[4,5,6,7]. Despite the degree of geometric complexity to which the multi-block technique has been usefully applied, it became obvious to the ARA development team during the latter half of the 1980s that practical limitations were being encountered as more complexity was being sought. It was decided that the route to enhanced complexity lay through the use of unstructured grids, based on their increased flexibility for this particular problem. However, rather than switch to a totally unstructured grid approach, a hybrid block-structured/unstructured grid approach was pursued, based on the desire to retain the efficiency, accuracy and user experience associated with structured grids in as much of the flowfield as possible. The extension of the multi-block method to encompass regions of unstructured grid resulted in the development of the SAUNA (Structured And Unstructured Numerical Analysis) CFD system.

The SAUNA system has recently undergone extensive validation and evaluation at the Euler equation flow modelling level and a number of inviscid simulations around complete aircraft have already been achieved[8,9]. Recent development of the system has focussed on the extension of the flow model to the Reynolds-averaged Navier-Stokes level. The progress to date has been in the implementation of a viscous flow capability on block-structured grids using an algebraic turbulence model with acceleration of the time-stepping to a steady state achieved through the use of a multi-grid technique. It is the main purpose of this paper to present an initial evaluation of this capability on a number of configurations.

A brief description of the SAUNA system is given in the following section, with details being cited to other references. Most detail is given to the flow algorithm, as this represents the new work being presented here, but again, for brevity, more details can be found elsewhere. The core of the paper is devoted to the results section. Three configurations are addressed on the theme of evaluation of the viscous flow modelling within SAUNA: a forward swept wing/foreplane geometry, with viscous effects on both lifting surfaces being included in the computations, an intake/S-bend diffuser geometry and a rectangular afterbody/nozzle geometry. Each is examined through comparison with both an inviscid flow solution and experimental data, in an attempt to assess the quality of the predictions. The emphasis is on demonstrating efficiency and accuracy over a wide range of geometrical and physical situations using a single CFD system. Finally, a few concluding remarks are made and a brief statement of current and future work on further development of the system is given.

Overview of SAUNA System

Grid Generation

SAUNA has three modes of grid generation, structured, unstructured and hybrid. The structured grid component is based on the multi-block approach which has been well documented over the past ten years[1,3,8]. The flow domain is automatically decomposed into a number of blocks, which are arranged so as to provide an optimum grid topology for each geometric component. The basic mesh generation on surfaces and in the field is performed using the elliptic equation approach. However, this technique is not ideally suited to generating grids for viscous flow simulation. Instead, the approach followed in SAUNA is first to create a mesh suitable for inviscid flow and then to refine the grid in the surface-normal direction within selected appropriate blocks using the transfinite interpolation technique. The option is present to select variable 'first cell height' over a wing surface, say, with required values at leading and trailing edges, tip and root being supplied. This procedure provides an efficient means (order minutes) of generating viscous meshes, given an initial inviscid mesh. The complete procedure is detailed in Reference 10.

The use of hybrid grids is aimed at complex configurations for which the structured mesh approach is inappropriate: this is normally judged by the unlikelihood of a high quality multi-block grid being able to be created within acceptable timescales. Initially, a structured grid is formed for a component subset of the desired configuration. A region is then removed based on geometric input and integrity with the complete configuration is achieved by adding component(s) within this void. The remaining voids are then filled with regions of unstructured mesh in a two-stage process. A buffer region composed of pyramids (to interface with the quadrilateral faces of the multi-block hexahedra) and tetrahedra is created first and subsequently an unstructured field grid of tetrahedra is generated using the Delaunay connection algorithm in tandem with an automatic point addition procedure. The complete approach offers a building-block route to creating meshes around vehicles of arbitrary complexity. In extreme cases, a completely unstructured grid may be required, but this is only advocated as a last resort within SAUNA for the reasons outlined in the introduction. Details of the generation of hybrid grids can be found in References 8, 11 and 12. An example of a hybrid grid on the surface of a generic transport aircraft is shown in Figure 1. Here, the geometrically complex part of the geometry, the pylon, is meshed using an unstructured grid region, while the remainder of the aircraft is enveloped by a block-structured mesh.

Flow Algorithm

The Navier-Stokes flow algorithm is of the vertex-storage finite-volume type and is based on the work of Jameson et al[13] and Radespiel[14]. The spatial discretisation of the inviscid terms in the flow equations reduces to a balancing of fluxes through the faces of overlapping control volumes, which are defined as being the union of all polyhedral elements (cells) which meet at a common vertex. Thus, within a structured block the control volume is composed of eight hexahedra, with a natural extension to all other grid regions. The viscous terms are computed using a two-stage process. Firstly, the stress tensor is evaluated at cell centres using Green's theorem applied to the surface of each cell. Secondly, viscous fluxes are balanced using an auxiliary control volume formed from the centroids of the individual cells which comprise the original control volume. Therefore, inviscid and viscous contributions to the governing Navier-Stokes equations are collected at a common vertex, but using differing control volumes. The full Navier-Stokes equations are addressed rather than a thin shear layer form. A zonal approach is followed whereby viscous effects are only included in grid blocks adjacent to selected solid surfaces and in

the ensuing wake regions.

An anisotropic dissipation model is used as datum, whereby scaling factors based on the wave speed for each individual grid edge and modified by cell aspect ratio are used in the edge difference accumulation process. The treatment of artificial dissipation is critical to obtaining accurate solutions to the governing equations, so that predictions are not corrupted by large non-physical effects. To this end, research has been, and is still being undertaken to further limit the magnitude of the dissipation terms below their datum level. Work by Hall[15] has assisted in this process to date, and modifications to the treatment of both the second and fourth order dissipation contributions at solid surfaces have been included in the calculations presented herein. Current emphasis is on reducing levels further within the main part of shear layers. A number of boundary conditions are available within SAUNA, including ones relevant to powered aircraft simulation (engine compressor face and jet efflux). The discretised equations are marched in time to a steady state using a 5-stage Runge-Kutta scheme with local time stepping, residual smoothing and, for inviscid simulations, enthalpy damping. For efficiency, the viscous terms are evaluated only at the first of the five stages and then frozen for the remaining stages. In addition, a multi-grid technique is used, currently for structured grids only. Convergence can be monitored by residual level or by stabilising of forces on selected components of the configuration.

The current level of turbulence modelling for viscous flow simulations is the Baldwin-Lomax algebraic model[16]. Modifications to the original model are made in the near-wake region to remove the discontinuity in the turbulent viscosity coefficient at the trailing edge. This is accomplished by phasing out the inner layer model gradually downstream of the trailing edge, rather than terminating it abruptly as in the original definition. It is believed that this treatment does not significantly increase the overall inaccuracies of the model in the wake region. Transition from laminar to turbulent flow is fixed in all the calculations described in this paper, defined either from experimental testing (roughness bands) if available or by estimates from an Euler solution. Again, a gradual phasing in of turbulence over, say, 5% local wing chord is normally applied. For cases in which more than one wake is present in a calculation, eg wing and foreplane, each individual wake is computed separately and, for the relevant case in this paper, is allowed to develop downstream independently (from the turbulence modelling viewpoint) of the other or of any nearby boundary layer. If it occurred that a wake would mix with another shear layer under normal circumstances, then some ad hoc treatment would have to be applied to the turbulence evaluation. Obviously, the Baldwin-Lomax model is not physically suited to such flows, and any such treatment would be developed purely on numerical rather than physical grounds.

Details of all aspects of the flow algorithm can be found in References 17, 18 and 19.

Results and Discussion

Three configurations are addressed below to demonstrate the viscous modelling capabilities of SAUNA. The quality of each Navier-Stokes prediction is assessed through comparison with an Euler prediction and experimental data.

Forward-swept Wing/Foreplane

The principal advantage of the SAUNA system is its ability to model accurately the flow around configurations whose aerodynamics are driven by an interaction between neighbouring geometrical components. To this end, a generic combat aircraft with multiple lifting surfaces (wing + foreplane) makes an ideal test case. Further, in relation to the present study, a configuration with forward sweep on the wing provides a test case where viscous effects are important even in predominantly attached flow, due to the strong influence of the foreplane on the inner part of the wing.

The geometry considered here is a research model[20]: the wing has leading-edge forward sweep of 30° over the outboard part, becoming unswept at the fuselage junction; the fuselage is based on a simple rectangular section with rounded corners and it expands over the axial extent of the wing intersection; a foreplane with a 45° aft-swept leading edge is also present, it is high mounted relative to the wing and has a setting of -3° for the cases considered here.

The Euler mesh used here, which took two man-days to generate, is almost identical to that used in Reference 9, so that 'C' grid topologies are used around lifting surfaces, embedded in a global Cartesian topology, with the blocks near to the body arranged to give a polar topology in the cross-flow plane with a spherical polar modelling of the nose region. The mesh contained 500K cells in total. Viscous effects are to be included on both lifting surfaces, so the Navier-Stokes mesh is

obtained by refining the grid around, and in the wake of, the wing and the foreplane. The grid in the direction normal to the blocks enclosing the foreplane shear layer is increased from 5 to 25, and that normal to the blocks enclosing the wing from 9 to 33, giving a total of 930K cells. For the flow case addressed below, this gives a value of the scaled boundary-layer coordinate y^+ of between 2 and 4 at the first grid points off the wing and foreplane surfaces. The surface mesh is shown in Figure 2.

As in Reference 9, one of the sustained manoeuvre design points for this configuration is examined, at $M_\infty = 0.9$, $\alpha = 5.8°$ and Reynolds number (based on mean aerodynamic chord) of 4.2×10^6. For this case, Navier-Stokes and Euler predictions are shown in Figures 3 and 4, compared with experimental data[20]. Transition is fixed at 5% local chord in both theory and experiment.

The flow on the upper surface of the forward-swept wing is dominated by a lift-induced shock on the outer wing. This merges with a shock caused by the presence of the bodyside, to give a strong inboard unswept shock with local Mach numbers of the order 1.35 immediately upstream of the shock. Over the majority of the wing upper surface, Euler and Navier-Stokes predictions are in close agreement with each other and with experimental data. The main viscous effects occur in the region of the shock wave, with a weakening and upstream shift being evident at all stations, as would be expected. Although a significant improvement is given by the viscous flow prediction, quantitative agreement with experiment has not been achieved, particularly at the most inboard station, where the experimental shock is somewhat weaker than the prediction.

On the wing lower surface, high quality agreement between all three data sets is obtained, except near the bodyside, where a strong inviscid flow suction peak prediction has been moderated by viscous effects, but not sufficiently to correlate closely with experiment.

The flow physics in the wing/fuselage junction region is highly complex and errors in the modelling technique are being introduced from a number of sources - eg lack of body shear layer, insufficient grid density, and turbulence modelling.

It is worth commenting at this point that the wing on this configuration is defined with both a thick trailing edge (0.4% local chord) and a slab-sided tip. Both these features are 'closed-down' in the grid generation within SAUNA, to give sharp edges in each case. This not only introduces a change to the model as tested but also introduces, in general, slope discontinuities. The pressure in the trailing edge region is well-predicted in the viscous flow model, but slight oscillatory behaviour can be observed, presumably caused, in part, by this geometry treatment. Oscillations of a similar nature have also been reported by Elsholz et al[21], for example. The flow in the tip region is obviously more important in terms of overall flow development for the present forward-swept wing than it would be for an aft-swept wing. The general high quality of predictions is indicative of a reasonable modelling strategy in this region.

Moving to the foreplane, similar comments are appropriate in terms of relative behaviour of Euler and Navier-Stokes predictions and overall solution quality. Again, the strong trailing-edge shock, formed due to the induced upwash of the wing, is not reproduced with high accuracy. Local Mach numbers ahead of this shock as high as 1.4 are observed, and the shock/boundary layer interaction may result in some separation, particularly in the wing/fuselage junction. Inadequacies in the turbulence modelling would give an error in the position of the unswept shock[22] which would, of course, be apparent as a greater percentage of the chord outboard. The trailing-edge oscillations are more severe on the foreplane than on the wing. The trailing edge is only marginally thicker on the foreplane (0.5% local chord), but the local mesh spacing is smaller leading to a steeper closing down of the trailing edge. This latter factor may be a prime cause of this increased spatial instability.

Intake/S-Bend Diffuser

The use of geometrically complex engine inlet ducts is common practice in modern military aircraft. S-shaped ducts are often used since the airframe-mounted inlet is not usually located on the central axis of the engine face. For high engine performance, an important requirement of the design of the duct is that the total pressure at the engine face is as uniform as possible, ie there is low engine face flow distortion[23,24]. However, engine frame weight and space limitations demand as short a duct as possible, resulting in high centre-line curvature and rapid changes in cross-sectional area. These geometric features can be responsible for the development of separation and strong secondary flow features, both of which increase the engine face flow distortion.

An idealised intake/diffuser geometry[25] is addressed here, as shown in Figure 5. It consists of an intake cowl of circular cross-section, joined smoothly to an S-bend diffusing duct of circular cross-section, which terminates at a circular engine face with an axisymmetric bullet at the centre. The topology of the block-structured grid generated around the geometry consists of C-grids around the cowl and bullet and a polar O-grid throughout the diffuser. A region of polar O-grid around the duct centre-line is replaced by a Cartesian topology to avoid cells of very small volume along the centre-line which, it is known, would adversely affect the convergence rate of the flow code[26,27]. Within the duct, the Euler grid had 87 points in the streamwise direction and 44 points in the normal direction giving a total of 103K points. The Navier-Stokes grid had 87 points and 68 points in the same directions and consisted of a total of 163K points. The first point away from the wall was placed at a distance where $y^+ \simeq 1$. To assess grid dependence, a finer Navier-Stokes grid which had a total of 288K points and consisted of 123 points and 100 points in the streamwise and normal directions within the duct was also generated. The results obtained on this grid did not differ significantly from those obtained on the coarser grid.

Comparisons of the surface pressure predictions with experiment[25,28] at $M_\infty = 0.21$ (Reynolds number of 0.84×10^6 based on maximum diameter) for two mass flow ratios (MFRs) are shown in Figures 6 and 7. The lower MFR case is shown in Figure 6, where it can be seen that the trend of the Euler prediction is similar to the Navier-Stokes prediction. However, the overall level of the surface pressures predicted by the Navier-Stokes calculation are significantly lower than the Euler predictions for the same MFR. This is caused by the boundary layers on the duct walls which create a blockage and lead to an increase in axial velocity external to the boundary layers, thus decreasing the engine face pressure. This change in engine face pressure is incorporated into the Navier-Stokes calculation by iteratively updating the outflow pressure boundary condition according to the change in effective exit area caused by the boundary layer development, while retaining consistency with the specified MFR. This iterative procedure is the main contributary factor in the superiority of the viscous results, although it is detrimental to the convergence rate. Overall, the Navier-Stokes predictions are in very close agreement with experiment in the throat region and the upstream part of the diffuser. Further downstream, the comparison on the starboard side, in particular, is not so close, where a local separation is indicated by the presence of a plateau in the experimental pressure distribution.

In Figure 7, the Navier-Stokes and Euler predictions are compared with experiment for the high MFR case. Although the Navier-Stokes predictions upstream and just downstream of the throat are again in very close agreement with experiment, the figure shows that the agreement is only qualitative throughout most of the diffuser. For this high MFR case, the viscous phenomenon known as vortex lift-off[23] dominates the flow field. This feature is characterised by the shedding of two counter-rotating vortices from the starboard side of the diffuser which are then convected downstream. These vortices are clearly visible in a qualitative fashion in the predictions on the engine face plane as shown by the vector plot in Figure 8. Such a complex secondary flow will cause a significant viscous blockage effect within the duct, and as is expected, the results in Figure 7 show that there is a greater difference between the Euler and Navier-Stokes predictions than for the low MFR case. The poor Navier-Stokes pressure predictions within the diffuser for the high MFR case may be attributed to the fact that this highly three-dimensional type of separated flow is well beyond the range of validity of the Baldwin-Lomax turbulence model. It is anticipated that a turbulence model of at least the two equation level of complexity would be required to adequately predict such a flow.

Rectangular Afterbody/Nozzle

The drag from the afterbody region of a typical fighter aircraft is a significant proportion of its total drag due to the occurrence of strong shock waves, large-scale viscous effects and separated flow. The afterbody presented here follows the definition of the NASA B4 wind-tunnel model[29]. It has a simple external geometry consisting of a conical nose, a body of constant, near rectangular cross-section and an afterbody, which waists down to a jet exit area which is 33% of the body's maximum cross-sectional area. The internal nozzle geometry is modelled completely from the circular duct at the turbine face through a constant area transition to a near rectangular section, to a convergent-divergent nozzle with planar sidewalls. Figure 9 shows the internal geometry as a shaded surface within the external wireframe geometry. Subtle geometry modifications mean that no base area exists with this computational model. The meshing strategy is to obtain a grid about the upper starboard quarter of the configuration due to the zero incidence, zero yaw flow conditions. A globally polar topology is used with an extra row

of blocks of Cartesian topology lying on the jet centre-line, in a similar fashion to the previous configuration. Viscous effects are considered on all solid surfaces. The first grid point spacing away from these surfaces is fixed at a constant value of 8.3×10^{-4} model inches (the total model length is 63 inches). The grid consists of 140K points in total with 49 points in the direction normal to the afterbody and 33 points in the direction normal to the nozzle. Figure 10 shows a detail of the grid on the vertical symmetry plane in the afterbody region. Euler results were obtained on similar grids with appropriately fewer points and larger cell spacings near solid surfaces.

Experimental data for two flow conditions have been used[29] at free-stream Mach numbers of 0.60 and 0.94. The flow at the lower Mach number condition is thought to be totally attached, whereas at the higher Mach number a strong shock wave is present on the afterbody with separated flow downstream of the shock. The Reynolds numbers are 17.3×10^6 and 21.0×10^6 (with respect to model length) for each flow condition, respectively. Both cases have a cold jet with a nozzle pressure ratio of approximately 4.0. Modelling the entirety of the external geometry allowed the boundary layer on the afterbody to form naturally, avoiding complex (and unknown) boundary conditions which would be required when considering an isolated afterbody.

The vertical symmetry plane ($Y = 0$) exhibits the most flow activity because the afterbody possesses its greatest boattail angle (17.6°) at this plane. Figure 11 shows the surface pressure coefficient distributions in this plane from the Navier-Stokes, Euler and experimental results for $M_\infty = 0.60$. The Navier-Stokes solution exhibits a marked improvement on the Euler calculation with a very good prediction of the magnitude of the suction peak and much closer agreement in the approximately linear pressure recovery region towards the afterbody trailing edge. Similar quality viscous results were observed at other cutting planes through the afterbody with less difference to the Euler results being observed at the afterbody side-wall where the boattail angle is less severe, and where the Euler results are generally closer to experiment. No evidence of flow separation was found in these Navier-Stokes results.

The results at the higher Mach number condition, $M_\infty = 0.94$, are depicted in Figure 12. This is a much more severe test of the computational method in that a shock-induced separation is the main feature of the flow. The Euler results are very poor in this region of the flowfield due to the prevalence of these gross viscous effects. Again, the Navier-Stokes results provide a good prediction of the magnitude of the suction peak and, at this plane, the prediction of the shock location is very good. On other cutting planes through the afterbody (not presented in the figures) shock locations slightly upstream of their experimental positions are noted, possibly indicating lack of sufficient grid density. Figure 12 shows that the pressures downstream of the shock are not calculated accurately. Towards the trailing edge the Navier-Stokes results agree more closely with the experimental values. Although the extent of separation is well predicted, it is believed that a more sophisticated turbulence model would yield better pressure results in the separation region, and would give a better representation of the mixing of the jet and external flows [30].

Flow Code Performance

The Navier-Stokes solver used in this study has a full multi-grid option. The time for one multi-grid cycle on the fine grid with three grid levels existing is, on average, 1.8×10^{-4} seconds per point on one processor of a CRAY2. The pressure distribution converges rapidly on the fine grid with around 200-400 cycles being required for graphical accuracy, for the levels of artificial dissipation set near a minimum required for spatial and temporal stability. The storage requirements for the solver are approximately 125 Words (64-bit) per point. Equivalent figures for the Euler solver are given in Reference 9.

Conclusions

This paper has focussed on the application of the CFD system with acronym SAUNA (Structured And Unstructured Numerical Analysis) to a variety of geometrical configurations. Emphasis has been given to the viscous flow modelling capabilities of the system, through solution of the Reynolds-averaged Navier-Stokes equations on appropriate meshes. Wide geometrical scope has been exemplified through the chosen test cases, thus highlighting the flexibility and efficiency of the block-structured mesh generation approach, to which the viscous flow option is currently limited. All grids used in this paper were generated in at most two days each.

The accuracy of the finite-volume vertex-storage flow solver has been demonstrated across a range of flow conditions. However, it must be stressed that what is presented here is no more than an

initial evaluation for each of the addressed configurations, the aim being to demonstrate the range of application rather than a statement of absolute accuracy. Quantitative agreement between viscous flow prediction and experiment has been demonstrated on parts of all the geometries examined here; a significant improvement of these predictions over those for inviscid flow is apparent elsewhere. The viscous meshes used here are certainly not fine enough to give definitive answers and if quantities in addition to pressure distributions are required with accuracy (eg wall shear, boundary layer thickness parameters) then a significant increase in density will be called for. This points to the importance of maximising accuracy on a given mesh through the careful control of artificial dissipation. The limitations of the Baldwin-Lomax turbulence model for some of the extreme conditions presented here are recognised, with current experience indicating that the generality of a Reynolds stress model is required to represent all relevant physical processes - in particular, flow separation arising from shock/boundary layer interaction. All these issues highlight the need for a continual improvement in the performance of computer hardware, with massively parallel processing appearing to be the route to follow in the future.

The main on-going development of SAUNA is in the area of viscous flow modelling in unstructured grid regions. Although the hybrid (structured/ unstructured) grid option in SAUNA receives little attention in this particular paper, it is this facet which makes the system unique and which allows high quality grids to be generated around configurations of arbitrary complexity in a balanced, flexible and efficient manner. Currently, only inviscid flow can be computed on such grids and in extending this to viscous flow, the difficult problem of generation of highly compressed unstructured grids must be addressed. Extensions to the turbulence modelling are also taking place up to and including the two-equation level.

Acknowledgement

This work has been undertaken with the support of the Procurement Executive, United Kingdom Ministry of Defence. The authors would like to thank their many colleagues for offering advice and helping in the production of this paper.

References

1 Weatherill, N P and Forsey, C R, 'Grid generation and flow calculation for complex aircraft geometries using a multi-block scheme', AIAA-84-1665, 1984

2 Weatherill, N P, Shaw, J A, Forsey, C R and Rose, K E, 'A discussion on mesh generation techniques applicable to complex geometries', AGARD CP-412, Paper 2, 1986

3 Shaw, J A, Georgala, J M and Weatherill, N P, 'The construction of component adaptive grids for aerodynamic geometries', Proc 2nd Int Conf on Num Grid Gen in CFD '88, Eds Sengupta et al, Pineridge Press, pp 383-394, 1988

4 Fulker, J L and Ashill, P R, 'A theoretical and experimental evaluation of a numerical method for calculating supersonic flows over wing/body configurations', AGARD CP-437, Paper 12, 1988

5 Stanniland, D R, Baxendale, A J and Carr, K G, 'The use of CFD methods to aid the aeodynamic design and analysis of wing/ pylon/store installations', Proc Royal Aero Soc Conf on Store Carriage Integration and Release, Bath, England, 1990

6 McParlin, S C, Doherty, J J and Wood, S E, 'Validation of a multi-block Euler method for supersonic flows about complex configurations', Proc 1993 European Forum on Recent Development and Applications in Aeronautical CFD, Paper 30, 1993

7 Fulker, J L, Ashill, P R and Shires, A, 'A theoretical and experimental investigation of the flow over a supersonic leading edge wing/body configuration', Proc 1993 European Forum on Recent Development and Applications in Aeronautical CFD, Paper 31, 1993

8 Shaw, J A, Peace, A J, Georgala, J M and Childs, P N, 'Validation and evaluation of the advanced aeronautical CFD system SAUNA - a method developer's view', Proc 1993 European Forum on Recent Development and Applications in Aeronautical CFD, Paper 3, 1993

9 Shaw, J A, Peace, A J, May, N E and Pocock, M F, 'Verification of the CFD simulation system SAUNA for complex aircraft configurations', AIAA-94-0393, 1994

10 Pocock, M F and Shaw, J A, 'Enhancements to a block-structured mesh generator for zonal viscous/inviscid simulations', ARA CR M237/8/2, 1994

11 Childs, P N, 'Generation of unstructured grids within SAUNA. Part 1: Surface grid generation', ARA Report 87, 1993

12 Childs, P N, 'Generation of unstructured grids within SAUNA. Part 2: Three dimensional field grid generation and boundary integrity', ARA Report 88, 1993
13 Jameson, A, Baker, T J and Weatherill, N P, 'Calculation of inviscid transonic flow over a complete aircraft', AIAA-86-0103, 1986
14 Radespiel, R, 'A cell-vertex multi-grid method for the Navier-Stokes equations', NASA TM 101557, 1989
15 Hall, M G, private communication
16 Baldwin, B S and Lomax, H, 'Thin layer approximation and algebraic model for turbulent separated flows', AIAA-78-257, 1978
17 Peace, A J and Shaw, J A, 'The modelling of aerodynamic flows by solution of the Euler equations on mixed polyhedral grids', Int J Num Methods in Eng, Vol 35, pp 2003-2029, 1992
18 Peace, A J, 'Multi-grid convergence acceleration of a cell-vertex Euler algorithm using block-structured meshes', ARA Memo 382, 1993
19 Peace, A J, 'A multi-grid Navier-Stokes method for block-structured meshes', ARA CR M237/8/4, 1994
20 Stanniland, D R, 'AGARD WG-14 Experimental Test Cases for CFD Validation', ARA Model Test Note M180/4, Volume 4, 1993
21 Elsholz, E, and Longo, J M A, 'Navier-Stokes simulation of a transonic wing-body configuration' Proc 1993 European Forum on Recent Developments and Applications in Aeronautical CFD, Paper 4, 1993
22 Marvin, J G, 'Turbulence modelling for computational aerodynamics', AIAA Vol 21, p 941, 1983
23 Anderson, B H, Reddy, D R, and Kapoor, K, 'A comparative study of full Navier-Stokes and reduced Navier-Stokes analyses for separating flows within a diffusing inlet S-duct', AIAA-93-2154, 1993
24 Harloff, G J, Reichert, B A, and Wellborn, S R, 'Navier-Stokes analysis and experimental data comparison of compressible flow in a diffusing S-duct', AIAA-92-2699-CP, 1992
25 'Air intakes for high speed vehicles', AGARD-AR-270, 1992
26 Shaw, J A, Peace, A J, and Forsey, C R, 'Inviscid solutions over an advanced combat aircraft including intake and jet effects using an Euler multi-block approach', ARA Memo 299, 1988
27 Harloff, G J, DeBonis, J R, Smith, C F, and Bruns, J E, 'Three-dimensional compressible turbulent computations for a nondiffusing S-duct', NASA CR 4391, 1992
28 Gibb, J, Private communication
29 Compton, W B, Data supplied to AGARD Working Group #17, 1993
30 May, N E, 'Evaluation of three turbulence models for transonic, axisymmetric afterbody/jet flows', Proc 2nd European Computational Fluid Dynamics Conference, Wiley, 1994

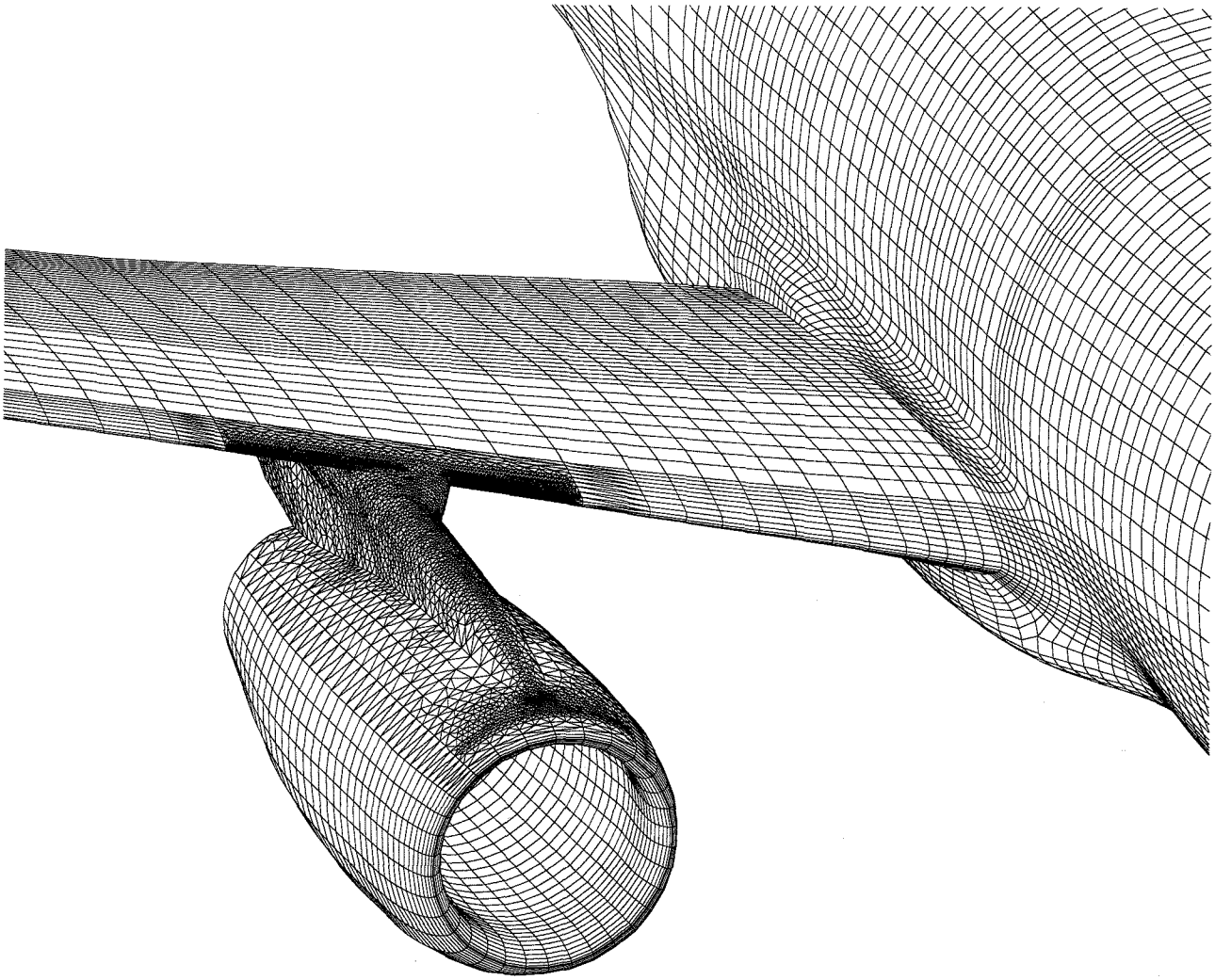

FIG 1 **Hybrid surface mesh on generic civil transport aircraft**

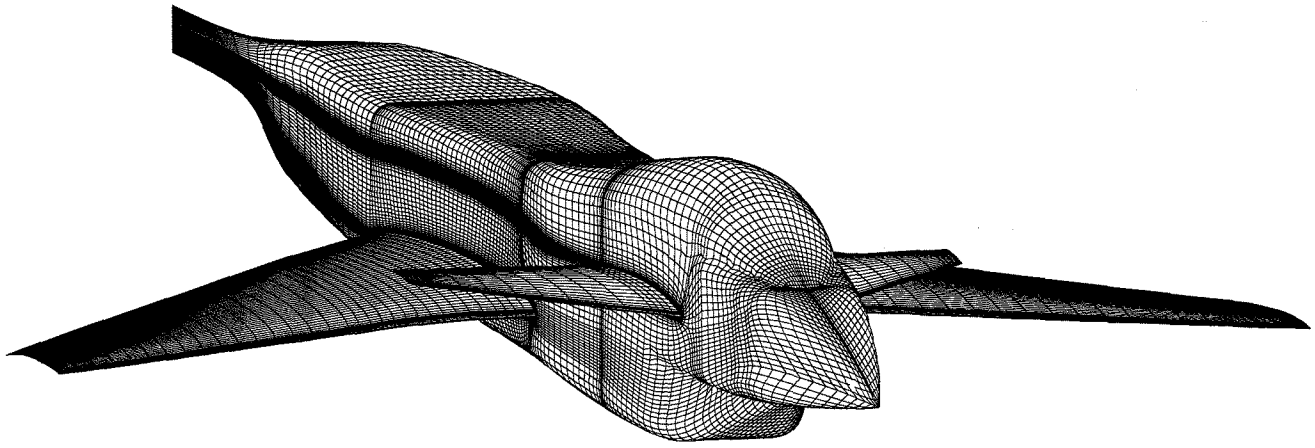

FIG 2 **Wing/body/foreplane surface mesh**

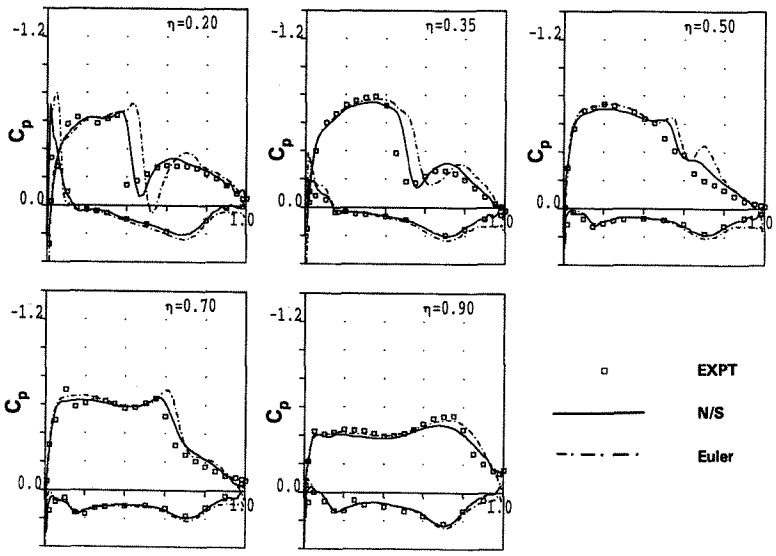

FIG 3 Wing/body/foreplane, wing pressures - $M_\infty = 0.9$, $\alpha = 5.8^0$

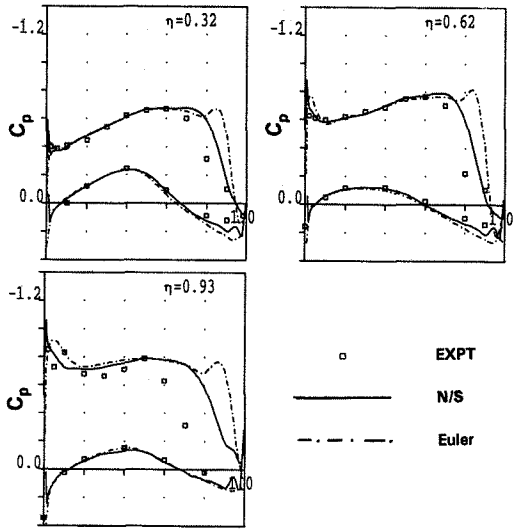

FIG 4 Wing/body/foreplane, foreplane pressures - $M\infty = 0.9$, $\alpha = 5.8^0$

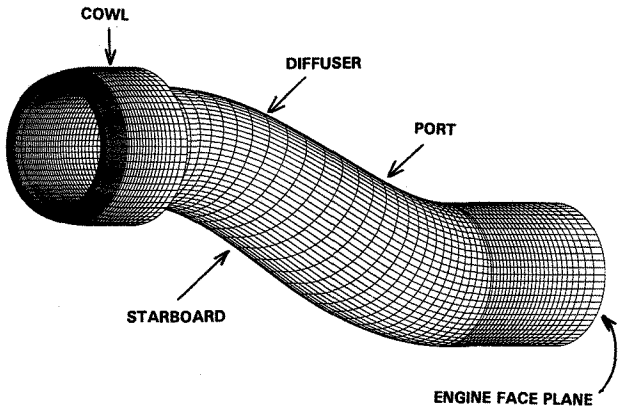

FIG 5 Intake/diffuser surface grid

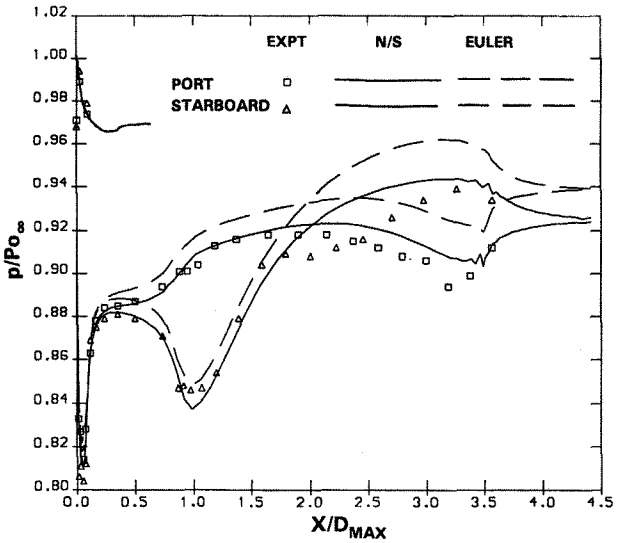

FIG 6 Intake/diffuser surface pressures - low MFR

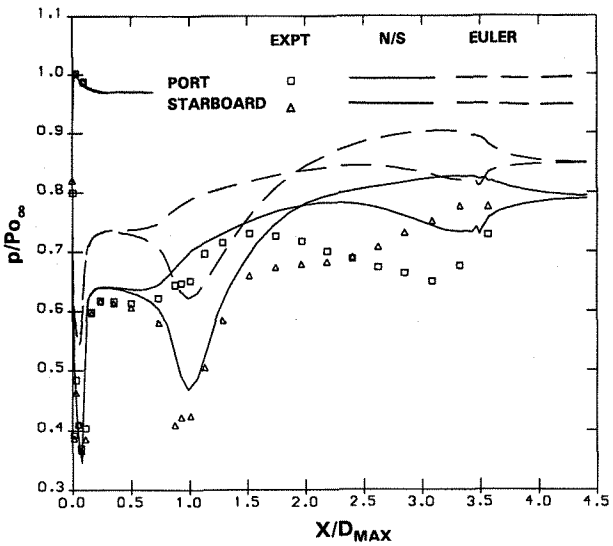

FIG 7 Intake/diffuser surface pressures - high MFR

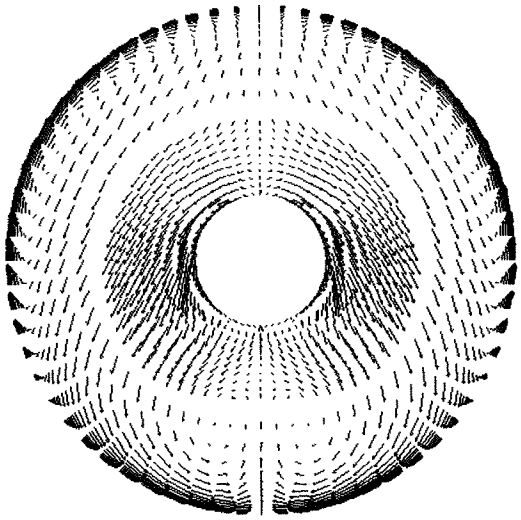

FIG 8 Engine face velocity vectors - high MFR

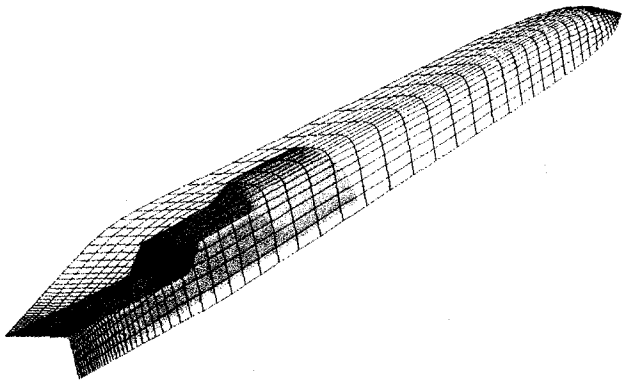

FIG 9 Afterbody model geometry

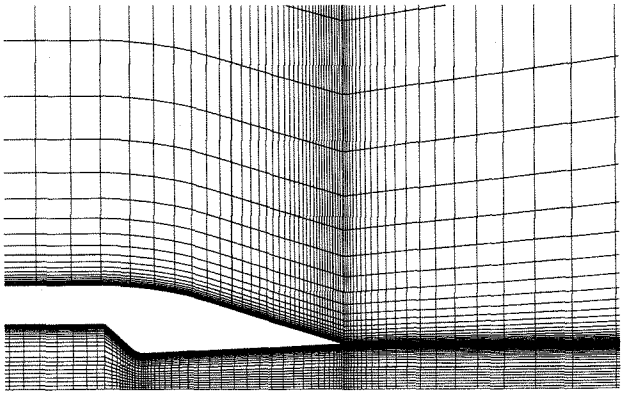

FIG 10 Afterbody grid on vertical plane

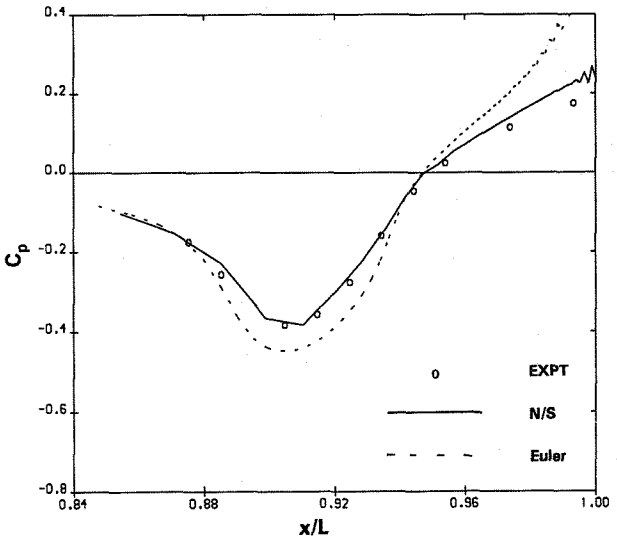

FIG 11 Afterbody surface pressures on vertical plane - $M_\infty = 0.6$

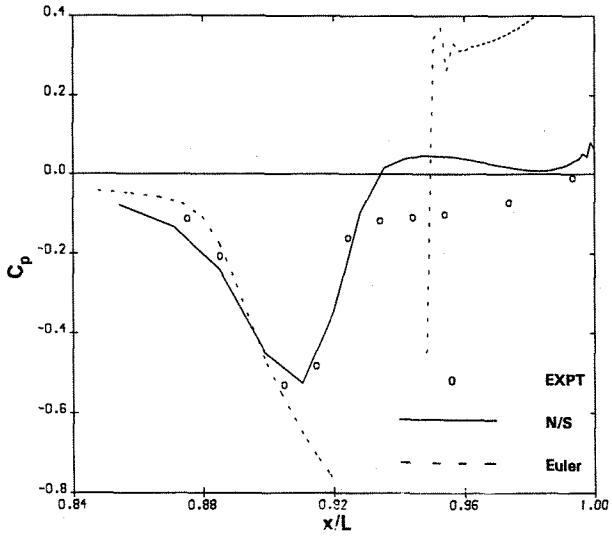

FIG 12 Afterbody surface pressures on vertical plane - $M_\infty = 0.94$